Proceedings of the Korean Nuclear Society Spring Meeting

Cheju, Korea, May 2001

A Digital Photographic Study on Nucleate Boiling in Subcooled Flow

In Cheol Bang[1], Won-Pil Baek[2], and Soon Heung Chang[1]

[1] Korea Advanced Institute of Science and Technology
373-1, Kusong-dong , Yusung-gu, Taejon, Korea 305-701

[2]Korea Atomic Energy Research Institute
150 Dukjin-dong, Yusong-gu, Taejon 305-353, Korea

Abstract

The behavior of near-wall bubbles in subcooled flow boiling has been investigated through digital visualization of water flow in vertical rectangular channels at atmospheric pressure. At subcooled and low-quality conditions, nucleation site density increases with the increases in heat flux and channel-averaged enthalpy, while discrete bubbles coalesce and form large bubbles, resulting in large vapor clots. Waves formed on the surface of the vapor clots are closely related to Helmholtz instability and CHF occurs in the procedure of repeated formation of the vapor clots. The liquid sublayer beneath large coalesced bubbles is identified photographically and tiny bubbles on the heated surface in the sublayer are also observed. Therefore, a flow nucleate boiling structure consists of the superheated liquid layer containing tiny bubbles, the flow bubble layer containing large coalesced bubbles over the superheated liquid layer and the liquid core over flow bubble layer. The CHF mechanism is related to the formation of large vapor clots due to coalescences of bubbles and dryout of the liquid sublayer.

1. INTRODUCTION

For the enhancement of energy transfer efficiency, forced convective nucleate boiling, which is preferred commonly by various heat transfer systems, is very effective in achieving high a heat flux with a small temperature difference between the heated surface and the cooling fluid. However, there is a boundary of the effective heat transfer regime, or DNB. This boundary has two faces of the highest heat transfer rate and the onset of heat transfer surface damage, and then is very important in that the damaging connect directly with the spread of radioactive materials in a nuclear power plant. However, the problem is that physical mechanism of this boundary is not understood clearly. This is mainly due to the fact that a detailed observation of the near-wall region at high heat and mass fluxes is very difficult.

Looking over the previous studies in high heat flux near and at DNB, following phenomena is mainly

reported.

(a) bubble crowding phenomena

(b) formation of vapor clot due to bubble coalescence

(c) vapor wave

In low pressure water tests, it is reported that bubble crowding and vapor clots were commonly observed.(Gunther 1951, Kirby et al. 1965) In high pressure R-113 tests, It is also reported that bubble crowding phenomena and phenomena forming a clump by coalescing of bubbles is mainly observed. Recently, in FC-87 and FC-72 tests, it is reported that vapor waves is newly observed. (Galloway and Mudawar(1993), Sturgis and Mudawar(1999)) This vapor wave is also due to vapor coalescences.

Through these observational reporting, how the DNB actually occur in the phenomena, the question has not generally solved yet. Just, various mechanisms have been reported as the causes of DNB but no theoretical models with good prediction performance are tightly linked to such visualization results. The objective of this study is to identify previously reported information through a visualization experiment and to give much clearer and advanced information for dubious parts of the phenomena. Recently flow visualization area has rapidly developed for the help of image technology development and new methods such as nuclear magnetic resonance technology and neutron radiography are applying to this area. Image technology area has advanced considerably for recent decades with the optical photographic technology and the digital technology. This would enable researchers to overcome some difficulties of visualization study for complex boiling phenomena. At this point, by using a digital imaging technology of photographic one, boiling phenomena and flow structure are investigated at subcooled conditions of water.

2. EXPERIMENTAL METHOD

2.1 Experimental loop

Visualization experiments for subcooled flow boiling have been performed with water at a pressure of 1.15 bar (T_{sat}=103 ^{o}C), for mass flux of 500, 1500, 2000 kg/m^{2}s and inlet subcooling of 50 ^{o}C. Figure 1

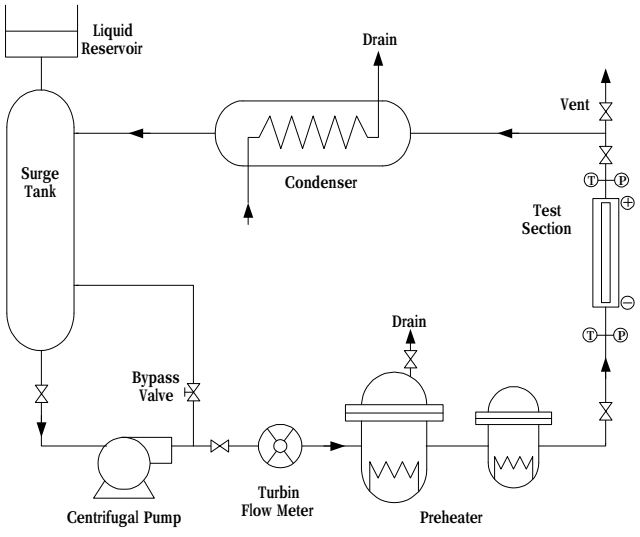

Fig. 1 Experimental Loop

shows the schematic of the experimental loop that consists of a centrifugal pump, a turbine flow meter, two preheaters, a test section, a condenser, a surge tank and a liquid reservoir.

Before performing tests, non-condensible gases dissolved in water were removed by pre-heaters in the way to keep the temperature 95 ^{o}C for an hour. After this work, auto temperature control unit of preheaters and a control of cooling water rate in a condenser keep subcooling 50 ^{o}C.

2.2 Test section for a flow boiling visualization

For the effective performance of flow visualization, test sections were designed the most suitably for the intensity of light. The basic structure and the characteristics are shown in figure 2. Test section has a type of vertically rectangular channel and consists of two major components of channel body and inserter with a heated plate and copper electrodes. The body is made of aluminum alloy and provides a flow channel of 8 mm*5 mm and polycarbonate windows for visualization at front and side parts. The inserter is made of Bakelite as an insulator and a stainless steel 304 heating plate with the size of 4 mm(width)*100 mm(length)*1.9mm(thickness). The plate is heated by the direct current which is supplied through copper electrodes connected at both ends.

The DC was supplied by means of a rectifier with the maximum power of 64 KW(32V, 2000A). The Bakelite insulator assures a sufficient insulation to allow only a negligible heat loss to surrounding air. In the figure 3, two thermocouples of a type of K are used to identify boiling curves and are located at the positions of 1 mm and 9 mm from the leading edge, and 0.4 mm in depth form the heated surface. Temperature is corrected through the equation $T_s = T(x) - \frac{fL}{2k}(1 - \frac{x^2}{L^2})$ acquired by a heat diffusion equation.(k : thermal conductivity, L : thickness of heater, ϕ : heat flux, x : distance from the inner)

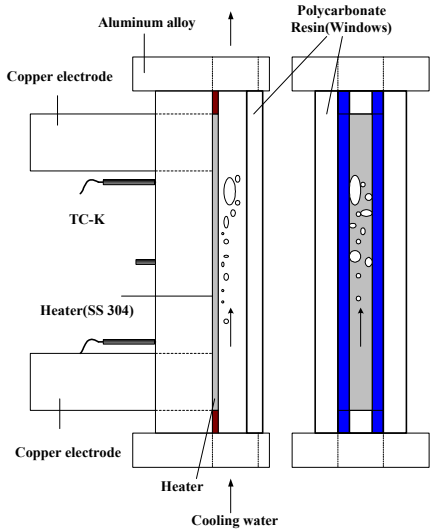

Fig. 2 Test Section

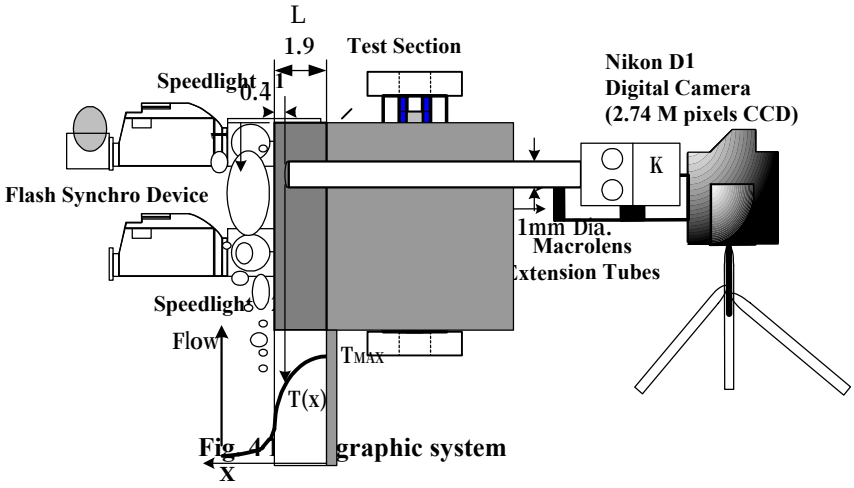

Fig. 3 Measurement of heater temperature

2.3 Visualization method

In the visualization of a flow channel, there are three determinate factors of an image storage method, the control of a exposure time, high a magnification.

In relation with image storage, the visualization is performed by the methods of both analog and digital techniques. As analog methods, 8 mm camcorder, still camera and high-speed camera are used. 8 mm camcorder is used to know overall phenomena of flow channel during a test and Kodak Ektapro 1000 motion analyzer as a high-speed camera was used. Images recorded at frame rates of 500 and 1000 fps have bad quality due to low resolution and low frame rate but it help to identify the movement paths of bubbles.

As a still camera, Nikon FM2 is used to acquire clear still images of moving bubble. It needs much time to fit the intensity of light properly and to develop a film where is a 35 mm analog film. To get rid of inefficiency of this experimental process, a digital camera was used.

As a digital method, Nikon D1 digital camera adopts Nikon F5 body and has 1/500 flash-synchronized speed, 2.74 Million pixel CCD instead of analog film, and flash memory. It also can interchange optical lens.

The use of this digital camera has many advantages of having no film developing procedure, identifying immediately photographic results and so on. These advantages enable to fit optical visualization conditions to grasp the intensity and surrounding conditions.

In another way with image storage method, it needs extremely short luminescence time to acquire clear still image. While the shutter is open (camera B-shutter) in the experiment, 1/8700 second of high-speed flash is emitted into flow channel. As the light source, two Nikon Speedlight SB-28 are used in single one and double flash method that needs a synchronizing device. Continuous photos have the time interval of 0.22 sec. In addition, an investigation through the photos, which are taken at relatively long exposure time, tries to distinguish flowing bubble and growing bubble.

Figure 4 shows this photographic system. Nikon 105 mm Macro lens and the three extension tubes of 14

mm, 21mm and 31 mm for the close-up is used to magnify the phenomena shown in flow channel. While focusing, the Halogen lamps of 2000 W and 300W as auxiliary light source are used. After the capture of fast moving bubble, image processing was performed mainly on the brightness and contrast of an image. For the exact measurements of bubble size and flow layer size, commercial image processing software of ImagePro Plus 4.1 is used.

In this works, visualization study has so far been focused not on a single bubble but on overall behavior of the bubble layer because the overall phenomena of flow structure are important in the viewpoint of flow boiling.

3. FLOW BOILING VISUALIZATION

The visualization was achieved respectively at the front and the sides of flow channel and simultaneously, indirect measurement of heated surface temperature was achieved to acquire a boiling curve. The partial observation of the flow channel is achieved to acquire large magnification observation of near-wall regions with large spatial resolution. On the other hand, the overall observation of the flow channel is performed to observe a distribution of bubbles and coalescence phenomena along a heated surface.

3.1 Boiling curves

In this study, boiling curves are acquired to know a generalization of observed boiling phenomena and to grasp relations between bubble behavior and heated surface temperature. These boiling curves as shown in figure 5 are compared with McAdams equation(1949) $h_l = 0.023\frac{k_f}{D_h}\left(\frac{GD_h}{m_f}\right)^{0.8}\left(\frac{C_p D_h}{k}\right)_f^{0.4}$ in single convective heat transfer region while those are compared with Jens and Lottes(1951) correlation $\Delta T_{sat} = 25f^{0.25}e^{-p/62}$ and Thom et al.(1965) correlation $\Delta T_{sat} = 22.65f^{0.5}e^{-p/87}$ in two-phase flow heat transfer region. As the result, these correlations predicted for a circular tube are comparatively consistent with the data of the experiments with rectangular channel in this study. Besides, while increasing mass flux, it is agreed such trends that heat transfer rate increases in single heat transfer region and mass flux effect is diminished in two-phase region. There were no outstanding changes of surface temperature due to bubble coalescence. Figure 6 shows sudden temperature rising at CHF.

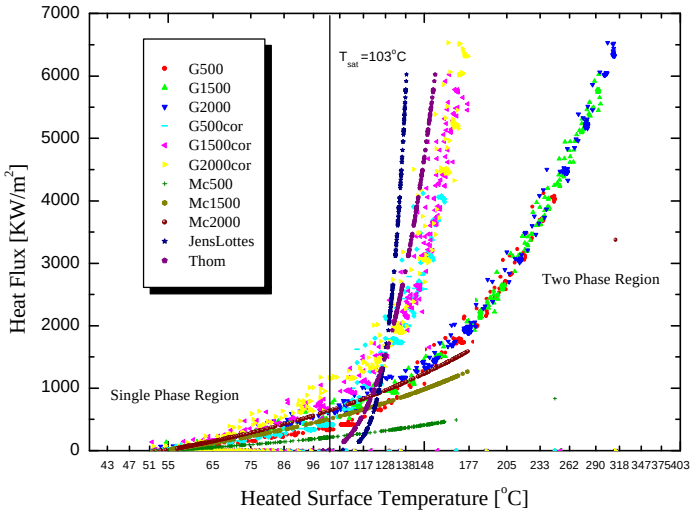

Fig. 5. Boiling Curves

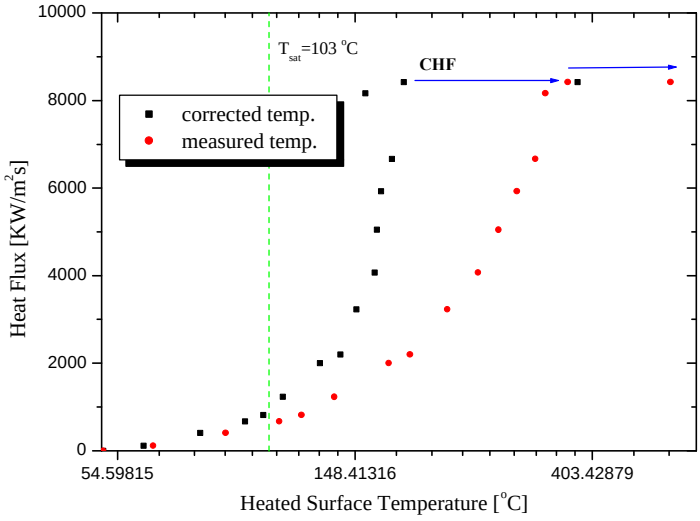

Fig. 6. Temperature rising at CHF

3.2 From Nucleation to bubble coalescence

For the partial heated surface, observational photos in the front and the sides of the test section were taken with change of mass flux in figure 7 and 8. In a range of low heat flux as shown in the figures, single phase heat transfer was first achieved and then in a range of heat flux over nucleation condition, discrete bubbles formed on heated surface are observed. While bubbles repeat to grow and decay, with the more increase of heat flux bubbles begin to move along the heated surface. The more increase of this moving bubbles and active nucleation sites with heat flux increase brings about bubble coalescences over

40% CHF as shown in photos. As the result of the coalescence of bubbles, large bubbles get formed. The large bubbles get formed large vapor clots due to more active nucleation sites over 80% CHF. These vapor clots are continually observed in relatively constant time interval. It is the reason that this vapor clots repeatedly forms on local heated surface according to nucleation site density and bubble frequency. The nucleation site density has the order of 10^6 nucleation/m^2 at high heat flux occurring bubble coalescences and increases with the increase of heat flux. Outstanding change by mass flux effect is that the dimension of bubbles decreases with the increase of mass flux. Bubble shape in side view has a hemisphere.

3.3 Superheated liquid layer below coalesced bubbles

Tong et al.(1966) begin to call the superheated thermal layer where tiny bubbles near wall exit as superheated liquid layer. However, photographic results are insufficient for this layer. As spoken above, more nucleation with heat flux increasing and the existence of tiny bubbles below vapor clot bring up the relationship with the existence of liquid sublayer that suggested in several CHF prediction models. The visualization experiments of this study produced the photos showing the superheated liquid layer like figure 9. There is a liquid layer with the size of a few dozens micron between large bubbles formed by bubble coalescence above 40% CHF and the heated surface. This is a reason that bubble coalescence do not make an effect on heated surface temperature. In figure 10, the non-uniform shadow formed over large bubble shows liquid layer transmitting the light emitted by the flash.

3.4 Critical heat flux

Vapor clots are frequently observed with the increase of heat flux and became larger by more coalescence. Figure 11 shows the observation for exit half heated surface with increase of heat flux. This shows bubble coalescence and the formation procedure of vapor clot in flow channel near wall. When 98% CHF is reached, vapor clots repeatedly are observed as shown in figure 12 of continuous photos with the time interval of 0.22 second. Early, bubbles form on heated surface and partially large bubbles are formed and then large vapor clot is formed. This vapor clot has the larger size than one formed in lower heat flux and the surface wave is observed on the surface of vapor clot. The wave is due to Helmholtz instability of becoming unstable by relative velocity difference between the passing liquid and vapor surface. This phenomenon is very important as a reason that the limit of vapor clot growth suggested in CHF prediction models is related to surface wave instability. The wavelength of the wave in this study is much shorter than the critical wavelength of Helmholtz instability that is large in low pressure generally. Its difference is due to no consideration of gravity and flow direction effect in critical wavelength equation. While vapor clots before approaching critical wavelength are diminished by a thermal limit of nucleation deactivation on heated surface related with insufficient supplying of vapor. This phenomenon is continued repeatedly.

A phenomenon at 100% CHF is shown in figure 13. The part of heated surface is damaged severely due to CHF occurrence and vapor clot and large bubbles is newly observed up and down for the damaged part. This is a reason that local heat transfer rate at damaged part where CHF occurred fell down sharply and the local heat was transferred by conduction to surrounding of CHF location.

Through the observation of these phenomena, a CHF mechanism is related to the dryout of liquid sublayer due to the formation of large vapor clot.

3.5 Flow nucleate boiling structure

Generally, when nucleate boiling occurs, it is known that the structure of flow layer is divided into a bubble layer and a liquid core, and there is a microlayer of liquid below each discrete bubble. Figure 14 shows the bubble layer and the liquid core well.

The phenomena shown through the visualization are considerably affected by light intensity and lighting direction. Figure 15 shows the observational results with the difference of the exposure time of flashing in the front. As shown in figure 14 a, the images of each discrete bubble in this bubble layer cannot give an averaged information because all bubble motions are in the state of freezing. Therefore, the investigation through extending a exposure time properly was performed for the continuous motions of discrete bubbles and coalesced bubbles in the layer as shown in figure 14 b. At relatively large heat flux(70% CHF), bubbles seems to be overlapped each other due to the increase of nucleation site density. The motions of bubbles seem to be dangling and separated from the heated surface and the orbits of faster separate bubbles in the liquid core than liquid are observed. In case of low heat flux, fine observation of near-wall phenomena is possible due to low nucleation site density as shown in figure 16. Long white lines are the traces of flowing bubbles which moved during the exposure time of 1/465 sec. Magnified image shows the liquid sublayer below the large vapor clot. There are tiny bubbles near wall and large bubbles right above. These large bubbles make a boundary between bubble layer and liquid core. It is regarded that they are in a layer because the size of tiny bubble is in a range of liquid sublayer dimension. Therefore, a flow nucleate boiling structure with three layers is suggested in this study as follows.

- The superheated liquid layer with very small bubbles attached on the heated surface
- The flowing bubble layer containing vapor clots and small bubbles(Coalescence occurs in this layer.)
- The liquid core over the flowing bubble layer

4. Conclusions

The behavior of near-wall bubbles in subcooled flow boiling has been photographically investigated with the help of recent digital imaging technology for water flow under atmospheric pressure. The main observational results are as follows:

(a) The number of activated nucleation sites increases with the increase in surface heat flux and channel-averaged local enthalpy;

(b) There is a liquid sublayer beneath large bubbles formed by coalescing of bubbles;

(c) The size of coalesced bubbles decreases with the increase in mass flux. Mass flux has no outstanding effect except for bubble size and layer thickness;

(d) At sufficiently high heat flux, about 80% CHF, the appearance of the vapor clot or blanket on the heated surface acts as an obstacle for liquid flow from the main liquid core region to the liquid sublayer near the wall;

(e) At sufficiently high heat flux, three characteristic regions are suggested on the basis of observations in the heated channel: (i) a superheated liquid layer with very small bubbles attached on the heated surface, (ii) a flowing bubble layer containing vapor clots and small bubbles, and (iii) the liquid core;

(f) At high heat fluxes near CHF, surface waves are observed on the surface of large vapor clot that is related to Helmholtz instability and limit of vapor clot growth

(g) The CHF occurred during the process of periodic formation of largely vapor clots and dryout of the liquid film near exit.

Acknowledgement

This work has been supported by Korea Atomic Energy Research Institute (KAERI) through research contract. Special thanks are given to Dr. M.K. Chung, Dr. S.K. Yang, and Mr. S.Y. Chun of KAERI.

5. REFERENCES

Celata, G.P., Cumo, M., Mariani, A. and Zummo, G. (1995). "Preliminary remarks on visualization of high heat flux burnout in subcooled water flow boiling", Two-phase flow modeling and experimentation, 859-866

Chang, S.H and Baek, W.P, (1997) ***Critical Heat Flux – Fundamentals and Applications***, Chungmoongak Pub. Co., Seoul, (in Korean)

Chang, S.H and Baek, W.P., (1997), "Perspective on critical heat flux research for reactor design and safety", NUTHOS-5, Beijing, China, AA1.

Chun, T.H., Baek, W.P. and Chang, S.H. (2000). "An Integral Equation Model for Critical Heat Flux at Subcooled and Low Quality Flow Boiling", Nucl. Eng. Des., Accepted for publication in 1999

Del Valle, Victor H. and Kenning, D.B.R. (1985). "Subcooled flow boiling at high heat flux", Int. J. Heat Mass Transfer, Vol. 28, No 10, 1907-1920

Fiori, M.P. and Bergles, A.E., (1970). "Model of critical heat flux in subcooled flow boiling", Proc. 4th Int. Heat Transfer Conf., Versailles, France, Vol. IV, p.B6.3.

Galloway, J.E. and Mudawar, I. (1993). "CHF mechanism in flow boiling from a short heated wall - I, Examination of near-wall conditions with the aid of photomicrography and high-speed video imaging", Int. J. Heat Mass Transfer, Vol. 36, 2527-2540

Gunther, F.C. (1951). “Photographic study of surface-boiling heat transfer to water with forced convection”, Trans. ASME, Vol. 73, 115-121

Ha, S.J. and No, H.C., (2000). “A dry-spot model of critical heat flux applicable to both pool boiling and subcooled forced convection boiling”, Int. J. Heat Mass Trasfer, 43, 241-250

Jiji, L.M. and Clark, J.A. (1962). “Bubble boundary layer and temperature profiles for forced convection boiling in channel flow”, Trans. ASME, J. heat transfer, 50-58

Kirby, G.J., Stainforth, R. and Kinneir, J.H., (1967). “A visual study of forced convection boiling – Part 2. Flow patterns and burnout for a round test section”, AEEW-R-506, UKAEA, Winfrith

Kureta, M. and Akimoto, H., (1998). “Experimental study on critical heat flux along one-side heated rectangular channel under subcooled conditions”, 6th ICONE-6226

Mattson, R.J., Hammitt, F.G. and Tong, L.S. (1973). “A photographic study of subcooled flow boiling and the boiling crisis in Freon-113”, ASME paper, 73-HT-39

Nariai, H., Kinoshita, H., Yoshida, T. and Inasaka, F., (1997). “Effect of tube length on the CHF of subcooled flow boiling”, 2nd Japanese-German Symposium on Multi-Phase Flow, Tokyo

Sturgis, J.C and Mudawar, I., (1999). “Critical heat flux in a long, rectangular channel subjected to one-sided heating-I. Flow visualization”, Int. J. Heat Mass Transfer 42, 1835-1847

Tong, L.S., Bishop, A.A. and Efferding, L.E. (1966). “A photographic study of subcooled boiling flow and DNB of Freon-113 in a vertical channel”, ASME paper, 66-WA/HT-3

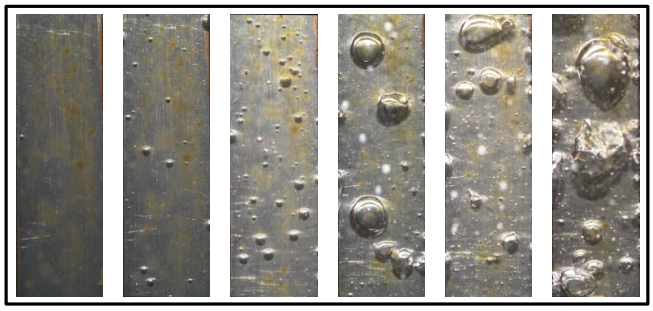

(a) Mass flux 500 kg/m²s

Area 4×13 m^2
0.334, 0.770, 1.13, 1.7, 2.45, 3.3 MW/m^2,
Quality (-x) =0.07769, 0.757, 0.07097, 0.06615, 0.05981, 0.05262

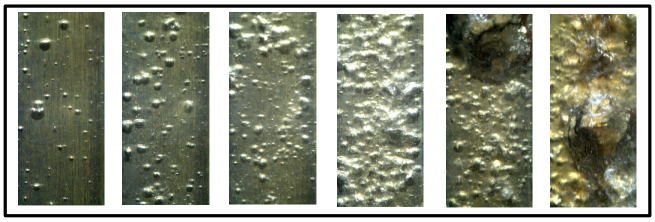

(b) Mass flux 1500 kg/m²s(6.4 MW/m^2, CHF)

Area 4×9 m^2
1.45 (22.7% CHF), 2.8 (43.8%), 4.5 (70.3%)
5.1 (79.7 %), 5.8 (90.6%), 6.3 (98.4%) MW/m^2
Quality (-x) = 0.0764, 0.0726, 0.0678, 0.0662, 0.0642, 0.0628

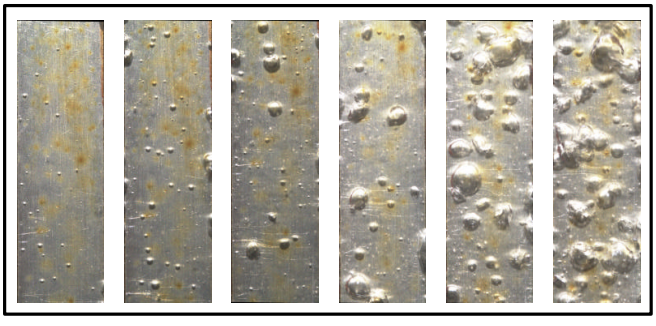

(c) Mass flux 2000 kg/m²s(8.4 MW/m^2, CHF)

Area 4×13 m^2, 1.77(21.1 % CHF), 2.4(28.6%), 3.23(38.5%),
4.8(57.1%), 5.8(69%), 7.0(83.3%) MW/m^2,
Quality(-x) = 0.7678, 0.7544, 0.7369, 0.7037, 0.06826, 0.06573

Fig. 7 Effect of heat flux on bubble behavior(Front)

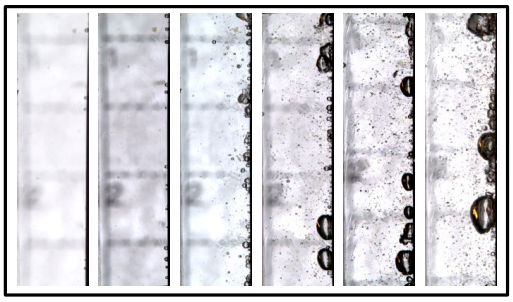

(a) Mass flux 500 kg/m²s

Area 5×20 m^2
0.333, 0.570, 1.154, 1.71, 2.4, 3.1MW/m^2,
Quality (-x)=0.0777, 0.0757, 0.07076, 0.06605, 0.06023, 0.05431

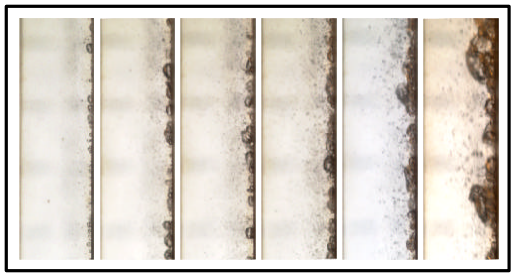

(b) Mass flux 1500 kg/m²s

Area 5×18 m^2,
2.0 (31% CHF), 3.2 (50%), 4.0 (63%),
5.0 (78%), 5.6 (88%), 5.9 (92%) MW/m^2,
Quality (-x) = 0.0749, 0.0715, 0.0693, 0.0664, 0.0647, 0.0639

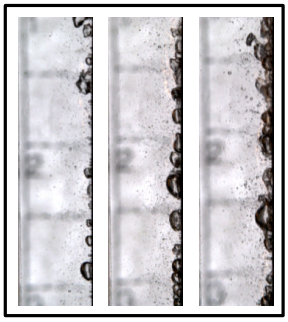

(c) Mass flux 2000 kg/m²s

Area 5×19 m^2
3.26(38.8%), 4.8(57.1%), 5.8(69%) MW/m^2,
Quality(-x) = 0.07363, 0.07037, 0.06826

Fig. 8 Effect of heat flux on bubble behavior(Side)

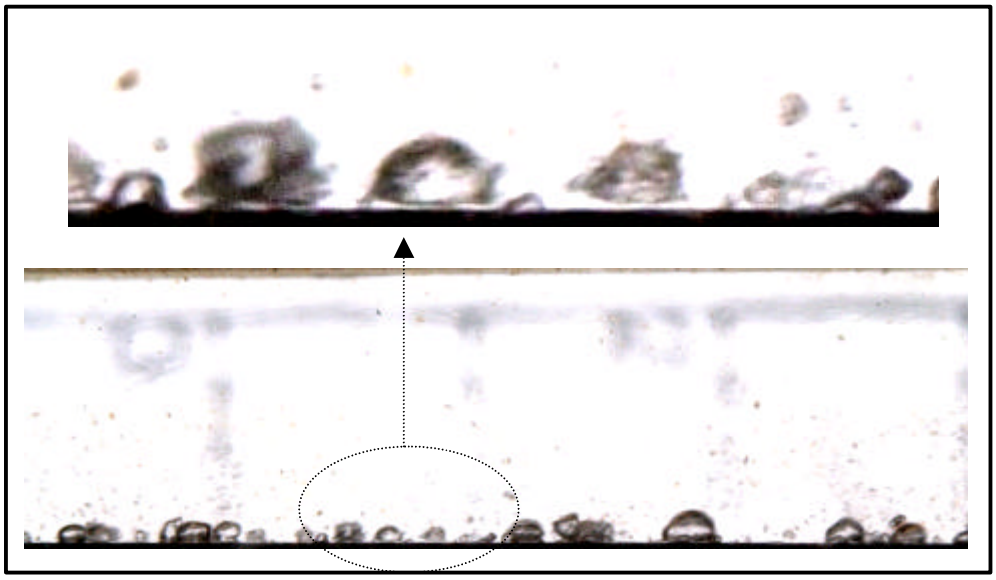

Fig. 9. Existence of liquid sublayer beneath large bubbles(Area 5´17.4 m^2)

Mass flux 2000 kg/m^2s, Heat flux 4.0 (48 % CHF) MW/m^2, Qaulity(-x)=0.07206

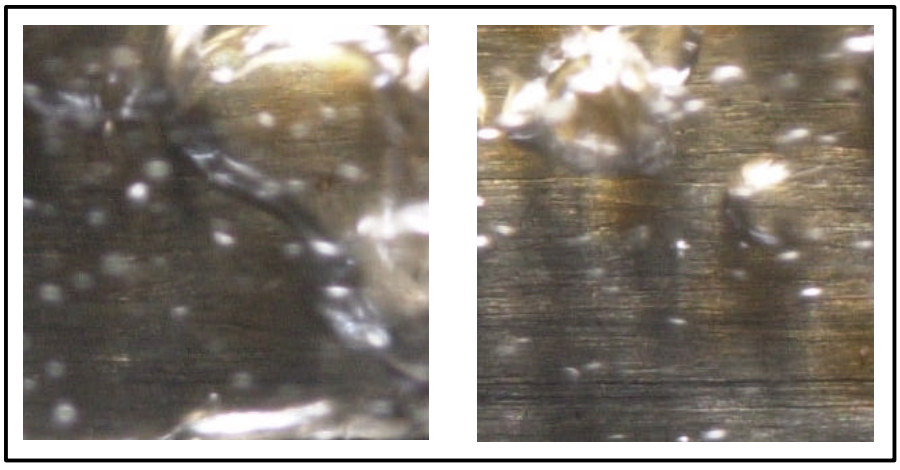

Fig. 10. Existence of liquid sublayer (Area 2´2 m^2)

Mass flux 2000 kg/m^2s, Heat flux 5.8 (69 % CHF), 7.0 (83.3 % CHF) MW/m^2,
Quality(-x)= 0.06826, 0.06573

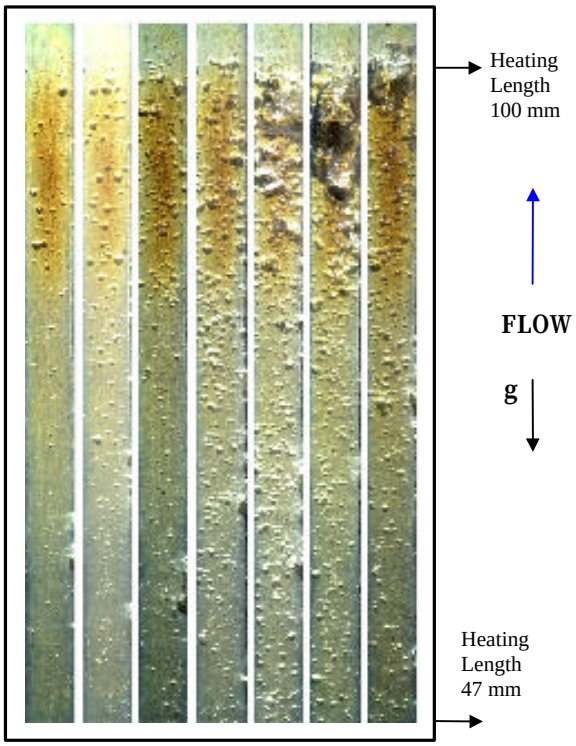

Fig. 11 Effect of heating length on bubble behavior

Area 4×60, 1500 kg/m^{2}s
(%CHF) 1.8 (28.1%) 2.4 (37.5%) 3.2 (50%) 4.0 (62.5%)
4.8 (75%) 5.3 (82.8%) 6.2 (96.9%) MW/m^2
Quality (-x) = 0.0754, 0.0738, 0.0715, 0.0693, 0.0670, 0.0656, 0.0631

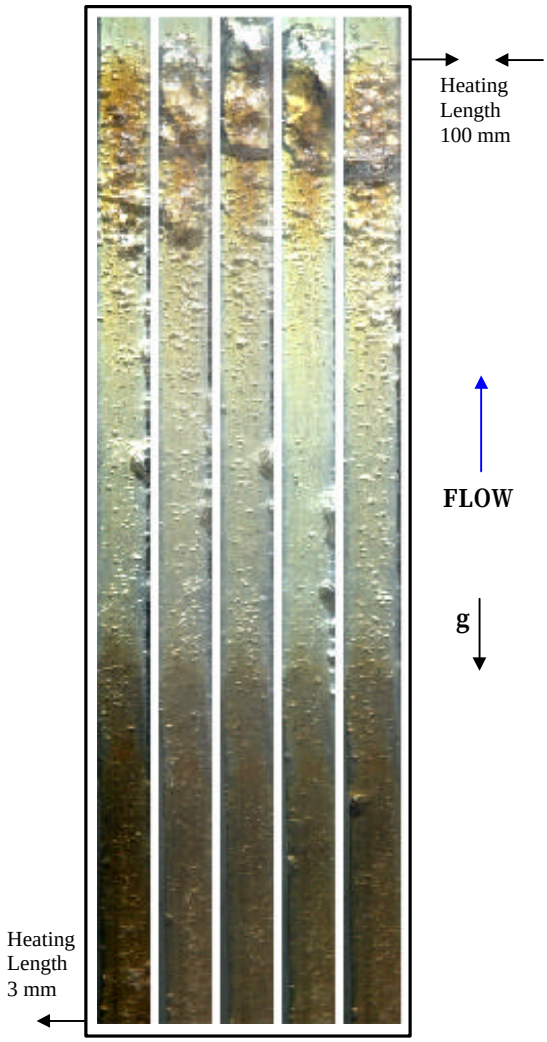

Fig. 12 Flow phenomena closely approaching DNB
1500 kg/m^{2}s
6.3(98.4%) MW/m^2
Quality(-x)=0.0628

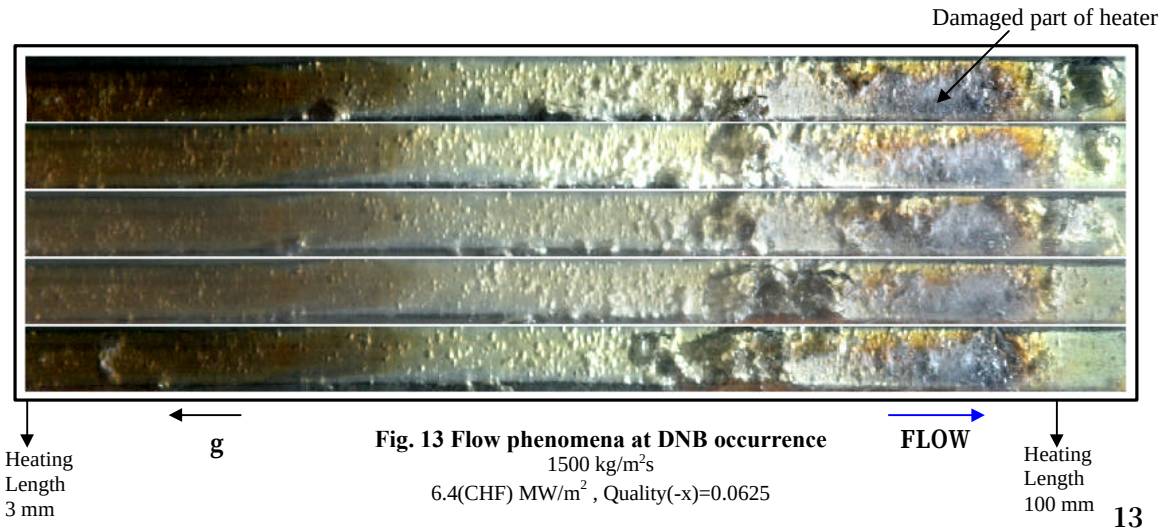

Fig. 13 Flow phenomena at DNB occurrence
1500 kg/m^{2}s
6.4(CHF) MW/m^2 , Quality(-x)=0.0625

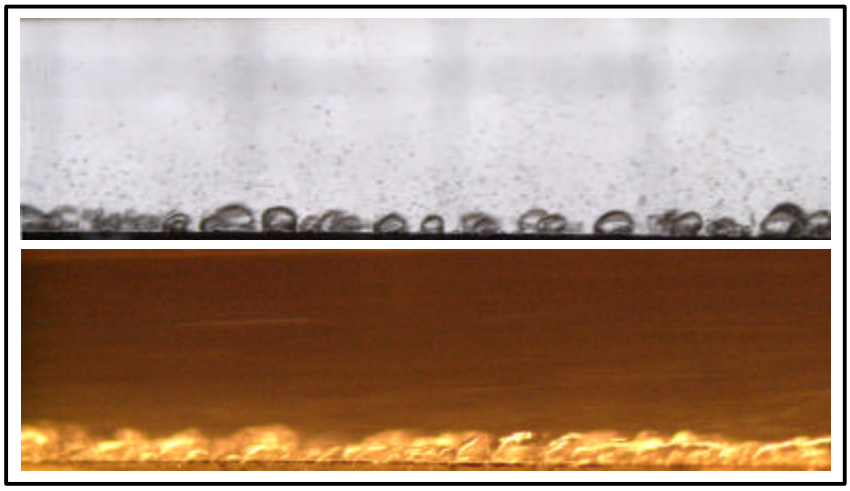

Fig. 14 Lateral views with different exposure times (Area 5*18.4 m^2)

(a) 1/8700 sec, (b) 1/500 shutter – 1/465 sec, Mass flux 2000 kg/m^2s, Heat flux 5.2 (70 % CHF) MW/m^2, (-x)=0.06953

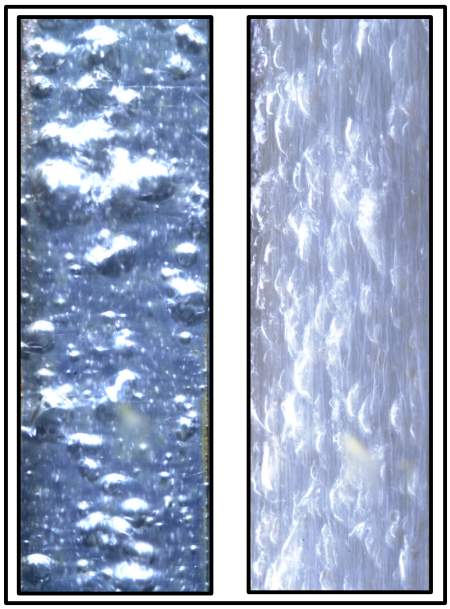

Fig. 15 Plan views with different exposure times

(a) 1/8700 sec, (b) 1/830 sec, Mass flux 2000 kg/m^2s
6.1 (73 % CHF) MW/m^2 ,(-x)=0.06763, (4mm width)

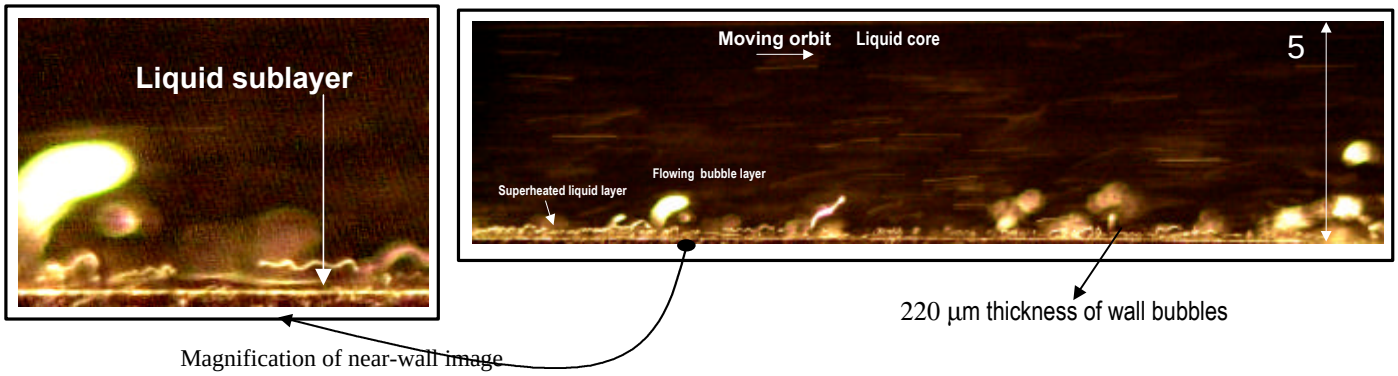

Fig. 16. Flow structure with three-layers

500 kg/m^2s, 2.0 MW/m^2, Quality (-x)=0.06361

1/500 shutter - 1/465 sec